Homonuclear ion-atom collisions: Application to Li^+-Li

N. Joshi,[1,*] M. Niranjan,[1] A. Pandey,[1,2] Olivier Dulieu,[2] Robin Côté,[3,4] and S. A. Rangwala[1,†]

[1]*Raman Research Institute, C. V. Raman Avenue, Sadashivanagar, Bangalore 560080, India*

[2]*Laboratoire Aimé Cotton, CNRS, Université Paris-Saclay, Orsay, 91400, France*

[3]*Department of Physics, University of Connecticut, Storrs, Connecticut 06269-3046, USA*

[4]*Physics Department, University of Massachusetts Boston, Boston, Massachusetts 02125, USA*

(Received 17 July 2021; revised 25 April 2022; accepted 6 May 2022; published 10 June 2022)

We present a theoretical framework for homonuclear, ground-state ion-atom collisions wherein the indistinguishability of direct elastic and resonant charge exchange (RCE) scattering channels is discussed. The discussion in terms of the total cross section($\sigma_{\rm tot}$) is motivated and derived. The standard cross-section expressions for direct elastic($\tilde{\sigma}_{\rm el}$) and RCE ($\tilde{\sigma}_{\rm ce}$) channels are obtained as high-energy approximations to $\sigma_{\rm tot}$. We show that the total cross section resolves the inconsistency, at low energies, between the diffusion cross section (σ_D) and the high-energy approximation to the total cross section ($\tilde{\sigma}_{\rm tot}$). The validity of the equivalence relation between the σ_D and $2\times\tilde{\sigma}_{\rm ce}$ is also discussed. The differences which result in cross sections which are frequently used in the description of ion-atom collision is illustrated with specific calculations for an Li^+-Li system. The use of $\sigma_{\rm tot}$ is advocated as a correct and consistent way to represent cross sections.

DOI: 10.1103/PhysRevA.105.063311

I. INTRODUCTION

Advances in cold dilute gas physics allow a large range of experiments. Among these, the study of collisions of a trapped ion in a dilute gas of trapped ultracold atoms is a rapidly growing area of interest [1–19]. Such experiments are performed in hybrid trap systems, where ions and atoms are confined with overlap. Here a single trapped ion can undergo binary [16] and ternary collisions [1,18,19] with the atoms. The present article focuses on collisions of the former type. In the energy regime where many partial waves contribute, binary ion-atom collisions can be reliably understood using a semiclassical description [11,20,21]. However, as the focus on the ultracold regimes of such interactions intensifies, a quantum formulation needs to be invoked.

In the particular case of homonuclear ion-atom collisions, there is inconsistency in literature with respect to how the binary collision cross sections, computed under the quantum formalism, are reported. This has happened as some high-energy approximations have been generalized to all regimes. The interpretation of the experiments which are under way now will be sensitive to the details of the cross section, so it is essential to have an unambiguous formulation in place. A collision between a homonuclear ion atom pair, which exhibits inversion symmetry, can occur via two collision channels, i.e., a direct elastic and a resonant charge exchange (RCE) channel. In a collision event, these channels are experimentally indistinguishable. Nevertheless, it is current practice to present independent cross sections for direct elastic and RCE channels for homonuclear ion-atom collisions [4,11,20,22–25]. In the low-energy limit, this separation of channels is invalid.

Here we revisit the theoretical formalism for homonuclear ion-atom collisions and derive the total binary collision cross section. This analysis closely follows the treatment of Massey and Smith [24,26,27]. We then obtain the standard expressions for direct elastic and RCE channels as high-energy approximations. Further, we show that the total cross section is equal to the diffusion cross section in the *s*-wave limit and discuss that at low collisional energies, no simple equivalence of the diffusion and RCE cross sections exists. The various relations are illustrated in the context of the Lithium ion-atom system. Finally, an average collision rate coefficient is evaluated for a range of temperatures.

II. Li^+–Li POTENTIAL ENERGY CURVES

For illustrating the discussion that follows, we shall consider $^6Li^+-{}^6Li$ and $^7Li^+-{}^7Li$ systems. For this purpose, we calculate here the nonrelativistic potential energy curves (PECs) for the symmetric($X^2\Sigma_g^+$) and antisymmetric ($A^2\Sigma_u^+$) electronic states of the $^6Li^+-{}^6Li$ system (see Fig. 1). The PECs for the $^7Li^+-{}^7Li$ system have been calculated in Pandey *et al.* [28]. For internuclear separations $R < 25.60a_0$, where a_0 is the Bohr radius, the ion-atom interaction energy is determined by the isotope independent *ab initio* PECs calculated in Ref. [28]. The *ab initio* PECs have been calculated using a body fixed coordinate system with the origin taken at the geometric center of the molecule. Beyond $25.60a_0$, the *ab initio* PECs are asymptotically extended. The ion-atom interaction potential is then calculated in terms of the induction energy $V^a_{\rm ind}(R)$ and exchange energy $V^a_{\rm exch}(R)$[28]. At very large internuclear distances, $V^a_{\rm exch}(R)$ is negligible and the interaction potential is well approximated by the leading

*njoshi@rri.res.in

†sarangwala@rri.res.in

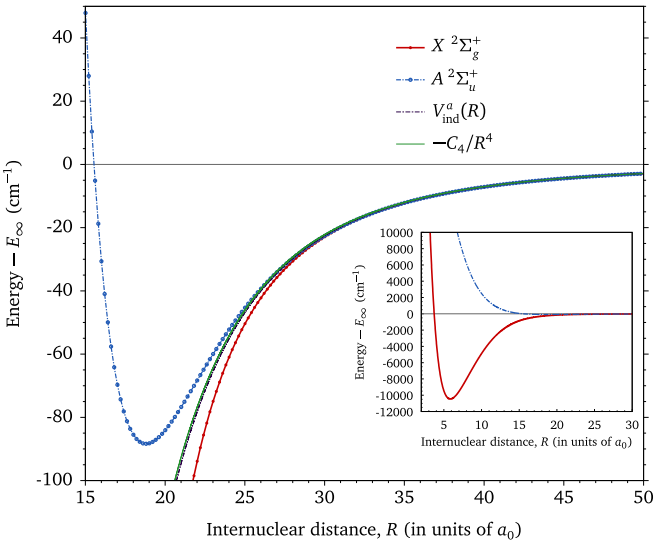

FIG. 1. The asymptotic limit of the first two states of $^6Li_2^+$, $X^2\Sigma_g^+$, and $A^2\Sigma_u^+$, calculated using the multireference configuration interaction (MRCI) method with aug-cc-pCV5Z basis set, are shown. Also shown are the induction energy $V_{\rm ind}^a(R)$ and $-C_4/R^4$. The dissociation limit, E_∞, is calculated by fitting the asymptotic form of the induction energy to the *ab initio* induction energy in the range $35a_0$ to $50a_0$. Further details can be found in Pandey *et al.* [28]. The figure and its inset depicts the minima of the $A^2\Sigma_u^+$ and $X^2\Sigma_g^+$ curves, respectively.

order term $-C_4/R^4$ of the induction energy $V_{\rm ind}^a(R)$, where $C_4 = \alpha_d/2$ and α_d is the static atomic dipole polarizability. The PEC's have been calculated under the Born-Oppenheimer (BO) approximation and are used in the discussion that follows. Effects of including the non-BO terms are discussed in the Appendix.

The full method for computation of the final scattering potentials was presented in detail in Ref. [28] and isotope specific details have been provided in Table I. The calculated scattering lengths for $X^2\Sigma_g^+$ and $A^2\Sigma_u^+$ states of $^6Li^+ - {}^6Li$ and $^7Li^+ - {}^7Li$ [28] are provided in Table II.

The doublet electronic states $X^2\Sigma_g^+$ and $A^2\Sigma_u^+$ are exhibited by homonuclear ion-atom systems where the atom has a single valence electron like in alkalis or two valence electrons like in alkaline earth species. As shown in Fig. 1, the states $X^2\Sigma_g^+$ and $A^2\Sigma_u^+$ are degenerate in the asymptotic limit. It is therefore equally probable for the collision to occur along either $X^2\Sigma_g^+$ and $A^2\Sigma_u^+$. Also, for homonuclear ion-atom systems, additional scattering outcomes manifest apart from direct elastic scattering. This is discussed in the following section.

TABLE I. Isotope specific parameters for ^{6}Li and ^{7}Li [28] that are used in preparation of the PECs, $X^2\Sigma_g^+$ and $A^2\Sigma_u^+$, for the scattering calculations. The static dipole, quadrapole, and octapole polarizabilities α_d, α_q, and α_o, respectively, are taken from Tang *et al.* [29]. All quantities are expressed in atomic units.

	α_d	α_q	α_o	Li_2^+ E_∞ (a.u.)
^{6}Li	164.169	1423.439	39654.460	14.756737566228
^{7}Li [28]	164.161	1423.415	39653.720	14.756737566693

TABLE II. $^6Li^+$-^{6}Li and $^7Li^+$-^{7}Li [28] scattering lengths computed for the states $X^2\Sigma_g^+$ and $A^2\Sigma_u^+$ are listed and compared with Zhang *et al.* [30] and Schmid *et al.* [31]. All quantities are expressed in atomic units.

$X^2\Sigma_g^+, A^2\Sigma_u^+$	a_g	a_g [30]	a_g [31]	a_u	a_u [30]
$^6Li^+ - {}^6Li$	−874	−918	−1014	−1355	−1425
$^7Li^+ - {}^7Li$ [28]	20465	14337	7162	1325	1262

III. HOMONUCLEAR ION-ATOM SCATTERING

First, let's consider the collision of an ion with a neutral atom such that they are of different elements or isotopes and both are in their respective ground states. Given the initial identification of the ion and atom, the postcollision outcome can be measured unambiguously. At low energies, where internal excitation of the colliding partners is energetically not possible, only direct elastic collisions occur. In this case, given a known initial configuration, whether the ion and the atom are forward scattered or backward scattered in the center of mass representation, is perfectly clear from the measurement of the scattering products. This is illustrated in Figs. 2(a) and 2(b), respectively. In contrast, for a homonuclear ion-atom system, due to the presence of inversion symmetry, other collision possibilities arise. In a collision, an electron can get exchanged from the atom to the ion, with no cost of energy, through RCE. The possibility of RCE which manifests in homonuclear systems can lead to collisions of the type illustrated in Figs. 2(c) and 3(d), in addition to direct elastic collisions. In any such collision, for the homonuclear case, it is in principle impossible to determine whether the charge has exchanged or not, making it problematic to distinguish between the direct elastic and RCE channels.

A. Total cross section

Since the collision happens along molecular ion PECs as shown in Fig. 1, the colliding homonuclear ion-atom pair can be described as two identical ion cores interacting in the presence of an active electron [27,32,33]. Whether the ion cores and/or nuclei are fermionic or bosonic determines the scattering outcome. Hence the overall wave function of the system is symmetric (for bosons) or antisymmetric (for fermions) under exchange of the ionic core and/or nuclei. Putting all this together, the asymptotic form of the wave function has been obtained by Massey and Smith [26,27], and the differential scattering cross section can then be written as [24,27,34]

$$I_{\rm tot}(\theta) = \frac{x}{4}|f_g(\theta) + f_g(\pi-\theta) + f_u(\theta) - f_u(\pi-\theta)|^2 + \frac{(1-x)}{4}|f_g(\theta) - f_g(\pi-\theta) + f_u(\theta) + f_u(\pi-\theta)|^2, \quad (1)$$

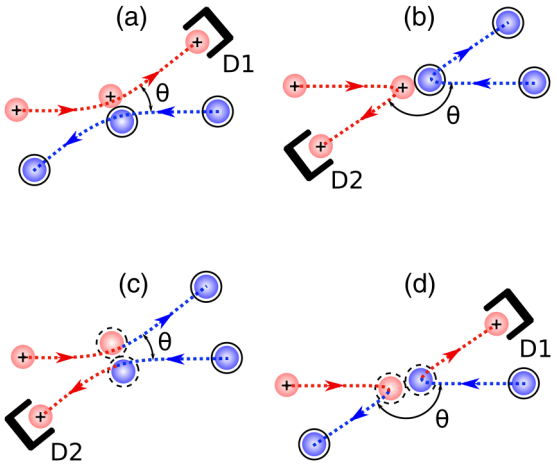

FIG. 2. Schematic representation of collisions is in the center-of-mass frame. The angle θ, in each panel, is defined as the deflection of the ion (or atom) from its initial trajectory had it just undergone direct elastic scattering and not RCE. Forward and backward ion-atom scattering scenarios without any change in the states of the colliding partners are illustrated in (a) and (b), respectively. The same scenario for the case where an electron is exchanged between the colliding partners, leading to charge swapping, is shown in (c) and (d). For a heteronuclear ion-atom system, only (a) and (b) are elastic and (c) and (d) become inelastic due to differences in the ionization energies of the two atoms. However, for a homonuclear ion-atom system, all four scenarios are elastic with (a) and (b) representing direct elastic and (c) and (d) representing resonant charge exchange (RCE) channels. Also, for the homonuclear case, (a) and (d) [(b) and (c)] cannot be distinguished leading to a superposition of both these processes for all collisions. Representation of collision with ballistic trajectories is just for the purpose of visualization.

where $x = (i+1)/(2i+1)$ for integer i (nuclear spin of the ion or atom) and corresponds to the case for bosons, whereas $x = i/(2i+1)$ for half integer i corresponding to fermions. Here f_g and f_u are the amplitudes for scattering along the electronic energy states $^2\Sigma_g^+$ or $^2\Sigma_u^+$, respectively.

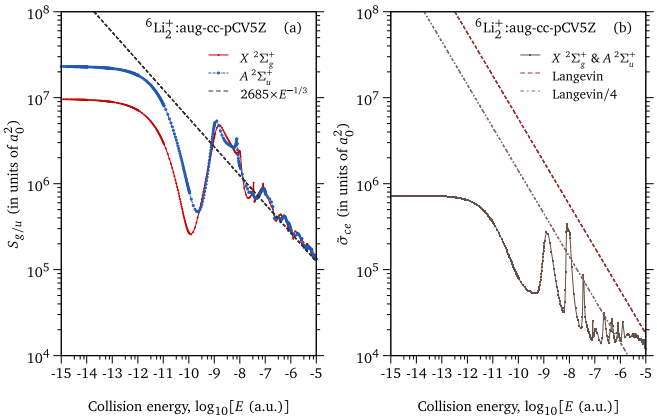

FIG. 3. $S_g(E)$ and $S_u(E)$ are compared with semi-classical total cross section in (a) and $\tilde{\sigma}_{ce}(E)$ is compared with the Langevin cross-section in (b), for $^6Li^+ - ^6Li$ collisions.

The differential scattering cross section can be conveniently written as

$$I_{tot}(\theta) = \frac{x}{4} I_1(\theta) + \frac{(1-x)}{4} I_2(\theta),$$

where $I_1(\theta)$ and $I_2(\theta)$ can be identified from Eq. (1) above.

The total scattering cross section is given by the expression

$$\sigma_{tot} = \iint I_{tot}(\theta) d\Omega = \frac{x}{4}\sigma_1 + \left(\frac{1-x}{4}\right)\sigma_2, \tag{2}$$

where $\sigma_1 = \iint I_1(\theta) d\Omega$, $\sigma_2 = \iint I_2(\theta) d\Omega$, and $d\Omega$ is the infinitesimal area element. The partial wave expansion for $f(\theta)$ and $f(\pi-\theta)$ is

$$f(\theta) = \sum_{\ell=0}^{\infty} \frac{(2\ell+1)}{k} P_\ell(\cos\theta) e^{i\eta^\ell} \tag{3}$$

and

$$f(\pi-\theta) = \sum_{\ell=0}^{\infty} \frac{(2\ell+1)}{k} P_\ell(\cos\theta)(-1)^\ell e^{i\eta^\ell}, \tag{4}$$

where ℓ is the angular momentum quantum number, $k = p/\hbar$, and η^ℓ is the phase shift. Using Eq. (3) and (4), we obtain

$$\sigma_1 = \frac{16\pi}{k^2}\left[\sum_{\ell=0,\text{even}\,\ell}^{\infty} (2\ell+1)\sin^2\eta_g^\ell + \sum_{\ell=1,\text{odd}\,\ell}^{\infty} (2\ell+1)\sin^2\eta_u^\ell\right] \tag{5}$$

and

$$\sigma_2 = \frac{16\pi}{k^2}\left[\sum_{\ell=1,\text{odd}\,\ell}^{\infty} (2\ell+1)\sin^2\eta_g^\ell + \sum_{\ell=0,\text{even}\,\ell}^{\infty} (2\ell+1)\sin^2\eta_u^\ell\right]. \tag{6}$$

The above expressions are obtained by using $\int_0^\pi P_\ell(\cos\theta) P_{\ell'}(\cos\theta)\sin\theta d\theta = \frac{2\delta_{\ell\ell'}}{(2\ell+1)}$, where $\delta_{\ell\ell'}$ is the Kronecker delta. Substituting Eqs. (5) and (6) in Eq. (2), we obtain the total cross section as

$$\begin{aligned}\sigma_{tot} = {} & x\frac{4\pi}{k^2}\left[\sum_{\ell=0,\text{even}\,\ell}^{\infty} (2\ell+1)\sin^2\eta_g^\ell + \sum_{\ell=1,\text{odd}\,\ell}^{\infty} (2\ell+1)\sin^2\eta_u^\ell\right] \\ & + (1-x)\frac{4\pi}{k^2}\left[\sum_{\ell=1,\text{odd}\,\ell}^{\infty} (2\ell+1)\sin^2\eta_g^\ell + \sum_{\ell=0,\text{even}\,\ell}^{\infty} (2\ell+1)\sin^2\eta_u^\ell\right].\end{aligned} \tag{7}$$

The above expression for the ion-atom cross section is valid from the lowest energies to well above thermal energies.

B. Consequences of high-energy approximations

In scattering events at relatively high collisional energies, significant angular asymmetry develops in the differential scattering cross section. As a consequence, $f(\theta)$ in Eq. (1) is

a decreasing function of θ and cross terms like $f(\theta)f(\pi-\theta)$ are small and can be neglected. On expansion and elimination of terms, there is a cancellation of the nuclear spin dependence. This yields the high-energy expression for the differential scattering cross section as

$$\tilde{I}_{\rm tot}(\theta) \approx \tfrac{1}{4}|f_g(\theta)+f_u(\theta)|^2 + \tfrac{1}{4}|f_g(\pi-\theta)-f_u(\pi-\theta)|^2. \tag{8}$$

At high energies, small angle scattering [Figs. 2(a) and 2(c)] is significantly more probable as opposed to large angle scattering [Figs. 2(b) and 2(d)]. Hence, if a charge detector D_1 detects an ion in the θ direction [i.e., Fig. 2(a)] it's most probably an ion which got scattered elastically in the forward direction. However, if the charge detector D_2 detects an ion in the $\pi-\theta$ direction [i.e., Fig. 2(c)], then it's most probably an atom which underwent forward elastic scattering accompanied by RCE. Therefore, in this situation, the term $(f_g(\theta)+f_u(\theta))/2$ can be identified as the direct elastic scattering amplitude and the term $(f_g(\pi-\theta)-f_u(\pi-\theta))/2$ is attributed to the scattering amplitude for RCE. The total cross section in the high-energy limit then becomes

$$\begin{aligned}\tilde{\sigma}_{\rm tot} &= \iint \tilde{I}_{\rm tot}(\theta)d\Omega = \frac{1}{2}(S_g(E)+S_u(E)) \\ &= \frac{2\pi}{k^2}\sum_{\ell=0}^{\infty}(2\ell+1)\big(\sin^2\eta_g^\ell + \sin^2\eta_u^\ell\big),\end{aligned} \tag{9}$$

where

$$S_p(E) = \iint |f_p(\theta)|^2 d\Omega = \frac{4\pi}{k^2}\sum_{\ell=0}^{\infty}(2\ell+1)\sin^2\eta_p^\ell, \tag{10}$$

$p \equiv g, u$ correspond to $X^2\Sigma_g^+$, $A^2\Sigma_u^+$, respectively, and the RCE cross section, $S_{\rm ce}$ [28], which is denoted by $\tilde{\sigma}_{\rm ce}$ here for notational consistency is

$$\tilde{\sigma}_{\rm ce} = \frac{\pi}{k^2}\sum_{\ell=0}^{\infty}(2\ell+1)\sin^2\big(\eta_u^\ell - \eta_g^\ell\big). \tag{11}$$

In this situation, the direct elastic cross section is defined to be

$$\tilde{\sigma}_{\rm el} = \tilde{\sigma}_{\rm tot} - \tilde{\sigma}_{\rm ce}. \tag{12}$$

$S_g(E)$, $S_u(E)$ and $\tilde{\sigma}_{\rm ce}(E)$ have been shown in Fig. 3 for $^6Li^+ - {}^6Li$. A comparison between $\sigma_{\rm tot}$ and $\tilde{\sigma}_{\rm tot}$ is made in Fig. 4 for the $^6Li^+ - {}^6Li$ and $^7Li^+ - {}^7Li$ systems.

In earlier work [24,34], the expression for $\tilde{\sigma}_{\rm tot}$, $\tilde{\sigma}_{\rm ce}$, $\tilde{\sigma}_{\rm el}$ in Eqs. (9), (11), and (12) has been identified as the total cross section, charge exchange cross section, and elastic cross section, respectively.

Clearly, such an identification can only be made in the high-energy limit. These approximations break down in the limit of low collision energies near the *s*-wave limit where the θ deflection angles are substantial and the scattering is increasingly isotropic. The presence of direct elastic and RCE cross sections is completely entrenched in literature [4,11,20,22–25,34] and the coming age of new experiments requires that these inconsistencies be recognized and corrected where required.

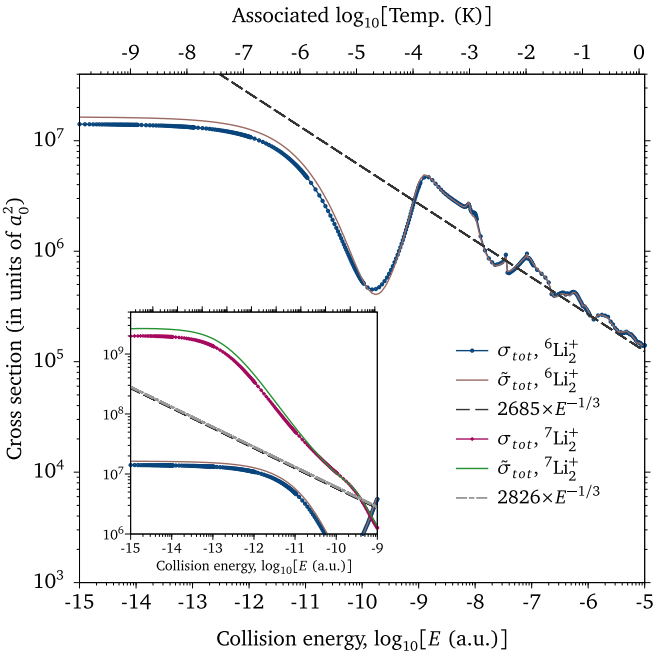

FIG. 4. $\sigma_{\rm tot}$ and $\tilde{\sigma}_{\rm tot}$ as a function of collision energies for $^6Li^+ - {}^6Li$ system. In the inset, differences between $\sigma_{\rm tot}$ and $\tilde{\sigma}_{\rm tot}$ in the s-wave energy regime are shown for $^6Li^+ - {}^6Li$ and $^7Li^+ - {}^7Li$.

The reason for prevalent discussion of approximate expressions in literature is rooted in early cross-beam experiments. In these, detection of the atom and/or ion in the forward direction of their respective incident beams after interaction was attributed to direct elastic collision and should the atom(ion), postcollision, be detected in the forward direction of the ion(atom) beam, respectively, the scattering was attributed to RCE [35]. This is the identification made after Eq. (8).

C. Diffusion cross section

The diffusion of an ion in a dilute gas of atoms is a measure of the deviation of the ion's position with time from its ballistic trajectory. It is also called the momentum transfer cross section as it quantifies the forward momentum lost by the ion. Here we are in the temperature and density limit where the diffusion is due to sequential binary collisions of the ion with the atoms in the gas. The expression for the diffusion cross section is given as [36]

$$\sigma_D = \iint (1-\cos\theta) I_{\rm tot}(\theta) d\Omega. \tag{13}$$

At low energies, large scattering angles are prevalent and, in the *s*-wave limit, the scattering becomes isotropic and $I_{\rm tot}(\theta)$ becomes a constant, i.e., independent of θ.

Therefore, the diffusion cross section becomes equal to the total cross section:

$$\sigma_D|_{E<E_p} = \sigma_{\rm tot}|_{E<E_p}. \tag{14}$$

Here E_p represents the height of the *p*-wave barrier of the ion-atom system. The general expression for the diffusion cross section is obtained by substituting Eq. (1) in Eq. (13)

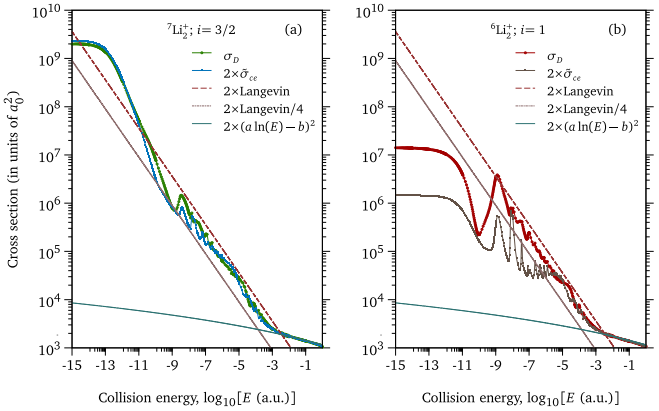

FIG. 5. Diffusion cross sections, σ_D, plotted for $^7Li^+ - {}^7Li$ in (a) and $^6Li^+ - {}^6Li$ in (b) and is compared with their respective $2 \times \tilde{\sigma}_{ce}$.

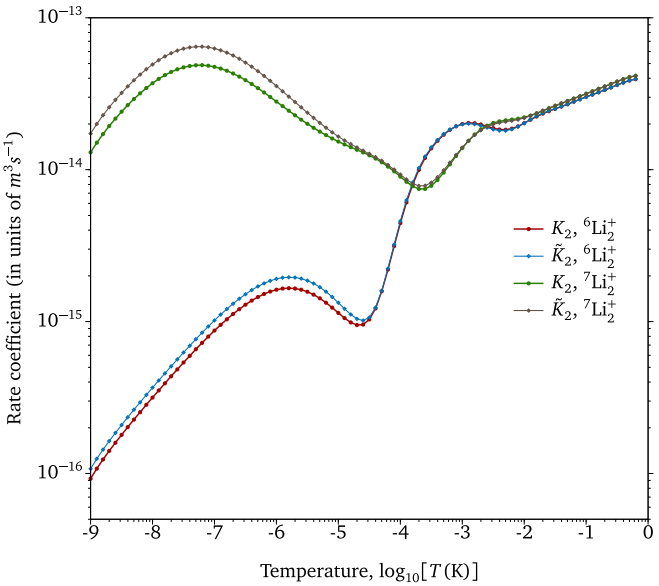

FIG. 6. The average collision rate coefficient plotted over a range of temperatures for both $^6Li^+ - {}^6Li$ and $^7Li^+ - {}^7Li$ systems.

and evaluating, which yields

$$\sigma_D = x\frac{4\pi}{k^2}\Bigg[\sum_{\ell=0,\text{even}\,\ell}^{\infty}(\ell+1)\sin^2\left(\eta_g^\ell - \eta_u^{\ell+1}\right) + \sum_{\ell=1,\text{odd}\,\ell}^{\infty}(\ell+1)\sin^2\left(\eta_u^\ell - \eta_g^{\ell+1}\right)\Bigg] + (1-x)\frac{4\pi}{k^2}\Bigg[\sum_{\ell=1,\text{odd}\,\ell}^{\infty}(\ell+1)\sin^2\left(\eta_g^\ell - \eta_u^{\ell+1}\right) + \sum_{\ell=0,\text{even}\,\ell}^{\infty}(\ell+1)\sin^2\left(\eta_u^\ell - \eta_g^{\ell+1}\right)\Bigg]. \quad (15)$$

σ_D, Eq. (15), becomes equal to σ_{tot}, Eq. (7), and deviates from $\tilde{\sigma}_{\text{tot}}$ in Eq. (9) in the ultralow-energy limits where the cross section is dominated by the contribution from the $\ell = 0$ term. In the high-energy limit, $\sigma_D \approx 2 \times \tilde{\sigma}_{ce}$.

We show a comparison between σ_D and $2 \times \tilde{\sigma}_{ce}$ in Fig. 5 for the $^6Li^+ - {}^6Li$ and $^7Li^+ - {}^7Li$ systems and discuss the condition for their general equivalence in Sec. IV.

IV. DISCUSSION AND CONCLUSIONS

$\tilde{\sigma}_{ce}(E)$ does not show Langevin-like behavior even for higher collision energies, which is the classical expectation for capture processes. Such deviation of the charge exchange cross section from the Langevin cross section can be expected when the scattering lengths a_g and a_u are comparable and of the same sign [37]. As a consequence, the phases of the states cancel out in the charge exchange cross-section expression, Eq. (11).

The total cross section, σ_{tot}, obtained by evaluating Eq. (7), is illustrated in Fig. 4 along with $\tilde{\sigma}_{\text{tot}}$ for $^6Li^+ - {}^6Li$, with $i = 1$, $x = 2/3$. It can be observed that for collision energies above 10^{-10} a.u., σ_{tot} and $\tilde{\sigma}_{\text{tot}}$ are identical. In the inset, we have shown σ_{tot} and $\tilde{\sigma}_{\text{tot}}$ for $^6Li^+ - {}^6Li$ and $^7Li^+ - {}^7Li$ systems in the ultracold energy limits. At 10^{-15}a.u., for $^6Li^+ - {}^6Li$, σ_{tot} is 12.33% less than $\tilde{\sigma}_{\text{tot}}$ whereas, for $^7Li^+ - {}^7Li$, σ_{tot} is 24.42% less than $\tilde{\sigma}_{\text{tot}}$. In the ultracold energy limit, the difference between σ_{tot} and $\tilde{\sigma}_{\text{tot}}$ is dictated by the nuclear spin and relative magnitude of a_g and a_u The difference will be enhanced when the nuclear spin is small and the magnitudes of a_g and a_u are very different. In general, the use of σ_{tot} as the total cross section has a significant impact on the cross-section accuracy.

The diffusion cross section, σ_D, obtained by evaluating Eq. (14), for $^6Li^+ - {}^6Li$ and $^7Li^+ - {}^7Li$ collisions is shown and compared with its respective $2 \times \tilde{\sigma}_{ce}$ in Fig. 5. In both cases, the correspondence among the peaks arising in the few partial wave regime can be observed. For $^7Li^+ - {}^7Li$, it is interesting that the equivalence relation between $2 \times \tilde{\sigma}_{ce}$ and σ_D holds well even at low energies near the s-wave limit. In the case of $^6Li^+ - {}^6Li$, $2 \times \tilde{\sigma}_{ce}$ compares well with the σ_D at high energies, above 10^{-5} a.u., but not at low energies. This illustrates that at low energies the equivalence relation does not hold for all homonuclear ion-atom systems. Therefore, in the context of calculating the diffusion [24,38] of an ion immersed in an ultracold cloud of its parent atom due to binary collisions, a scaling cannot be assumed between σ_D and $\tilde{\sigma}_{ce}$ in general.

For an ion and atom in thermal equilibrium at temperature T, the average collision rate coefficient corresponding to σ_{tot} and $\tilde{\sigma}_{\text{tot}}$ is given by $K_2 = \langle\sigma_{\text{tot}}v\rangle_T$ and $\tilde{K}_2 = \langle\tilde{\sigma}_{\text{tot}}v\rangle_T$, respectively, where v is the relative ion-atom speed. This is plotted in Fig. 6 for both the $^6Li^+ - {}^6Li$ and $^7Li^+ - {}^7Li$ systems.

We have used the BO-PECs so far for illustrating the scattering discussion. The non-BO matrix elements [39,40] are nonzero in the coordinate system that we have used to calculate the PECs. The effects arising due to their inclusion are discussed in the Appendix. However, the relations between the various cross sections and the qualitative conclusions reached are unaffected by their inclusion.

It is clear that the deviation between σ_{tot} and $\tilde{\sigma}_{\text{tot}}$ is maximum in the s-wave limit and decreases quite rapidly as nonzero partial waves start contributing with increasing collision energies. The cross section with accurate expression for the previous work can be evaluated if the phase shifts for the collision parameter space (ℓ,E) is available along with

the correct spin dependence of the ion core and/or nuclei. For experiments at high energies [20], the approximations are robust and the experimental results which depend on $\tilde{\sigma}_{\rm el}$ and $\tilde{\sigma}_{\rm ce}$ remain unchanged in their interpretation. In the future, as experiments with homonuclear ion-atom systems move to low collisional energies, adopting the correct formalism is essential for both the qualitative and quantitative understanding of the physics of these systems.

ACKNOWLEDGMENTS

The authors acknowledge support from IFC-PAR/CEFIPRA Grant No. 5404-1, Ministry of Electronics and Information Technology (MeitY), Government of India, under a Centre for Excellence in Quantum Technologies grant with Ref. No. 4(7)/2020-ITEA and the National Science Foundation Grant No. PHY-2034284 (R.C.).

APPENDIX: EFFECT OF NON-BO TERMS ON THE SCATTERING LENGTHS

In the main body of the article, the $X^2\Sigma_g^+$ and $A^2\Sigma_u^+$ PECs of Li_2^+, and the corresponding scattering properties, are computed without the non-BO terms in the Schrödinger equation. In this Appendix, we calculate these terms, namely, the diagonal BO correction, (DBOC), which in its first order is given by

$$\mathrm{DBOC}(R) = \langle 1^2\Sigma_p^+ | \sum_A \frac{-\hbar^2}{2M_A}\nabla_A^2 | 1^2\Sigma_p^+\rangle, \qquad \text{(A1)}$$

and the nonadiabatic coupling matrix elements (NACMEs) for the potentials with their first excited states,

$$\mathrm{NACME}(R) = \langle 1^2\Sigma_p^+ | \partial/\partial R | 2^2\Sigma_p^+\rangle, \qquad \text{(A2)}$$

where $p \equiv g, u$.

The DBOC for $X^2\Sigma_g^+$ states for $^7Li_2^+$ and $^6Li_2^+$ are computed with the CFOUR program at the coupled cluster-single, double excitation (CCSD) level with Widmark-Malmqvist-Roos basis sets [41]. Calculations are performed for the internuclear distances from $2a_0$ to $50a_0$. When $R \simeq 50a_0$, the absolute value of the DBOC term is almost constant [equal to 258.9917 cm^{-1} and 302.0982 cm^{-1}, for $^7Li_2^+(X^2\Sigma_g^+)$ and $^6Li_2^+(X^2\Sigma_g^+)$, respectively], varying by $\sim +0.0001$ cm^{-1} between $49a_0$ and $50a_0$. The change of DBOC(R) with respect to DBOC($R = 50a_0$) is shown in Fig. 7. The vertical line at $R_{\rm in} = 3.713a_0$ represents the position of the repulsive wall of the $X^2\Sigma_g^+$ PEC at zero (ultracold) kinetic energy. At equilibrium distance, $R_e = 5.85a_0$, the variations of DBOC with respect to its value at $50a_0$ are -0.1344 cm^{-1} and -0.1568 cm^{-1}, for $^7Li_2^+(X^2\Sigma_g^+)$ and $^6Li_2^+(X^2\Sigma_g^+)$, respectively. For $R > R_e$, the largest variation of the DBOC is observed at $R \sim 9a_0$, equal to -0.9792 cm^{-1} and -1.1422 cm^{-1} for $^7Li_2^+(X^2\Sigma_g^+)$ and $^6Li_2^+(X^2\Sigma_g^+)$, respectively. As a verification these DBOC corrections are $\approx (m_e/M)\times$BO-PECs, where m_e is the electron mass and M is the nuclear mass.

The NACMEs are calculated at the MRCI level with aug-cc-pCV5Z basis sets using MOLPRO package [43]. The corresponding energy corrections, calculated using the virial theorem, are shown in Fig. 8(a). Figures 8(b) and 8(c) show

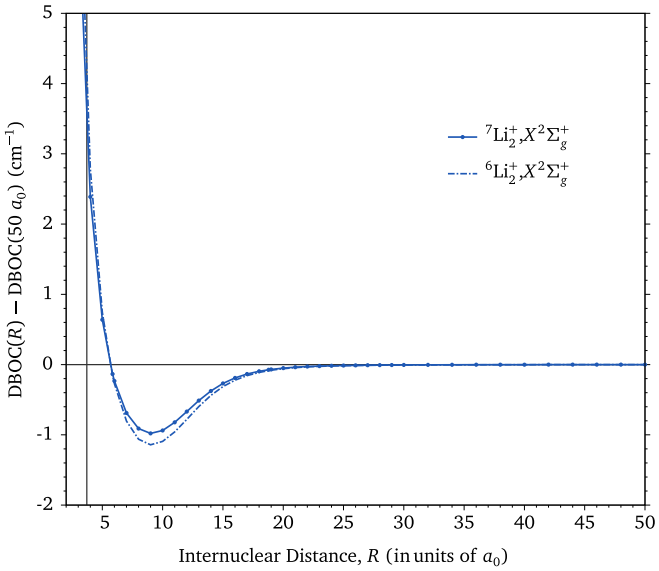

FIG. 7. DBOC, computed at the CCSD level, for $^6Li_2^+, X^2\Sigma_g^+$ and $^7Li_2^+, X^2\Sigma_g^+$ relative to their value at $R = 50a_0$.

the $\beta(R)$ parameter (Eq. (3) in Ref. [42]) and the NACME terms $\langle 1^2\Sigma_g^+, |\partial/\partial R| 2^2\Sigma_g^+\rangle$ and $\langle 1^2\Sigma_u^+ | \partial/\partial R | 2^2\Sigma_u^+\rangle$, respectively, used for computing the energy corrections. The correction for the relevant R range for $X^2\Sigma_g^+$, i.e., $R > R_{\rm in}(=3.713a_0)$ is less than $+0.3$ cm^{-1}. For $A^2\Sigma_u^+$, for $R > R_{\rm in}(=15.540a_0)$, the correction is less than $+0.003$ cm^{-1}.

As reported in Ref. [28] on the scattering length calculations of $^7Li_2^+$, the R-dependent relativistic corrections are less than -1.00 cm^{-1} for $R > R_e$ and less than -5.00 cm^{-1} for $R < R_e$, where R_e is the well depth position. The basis set superposition error, BSSE, calculated with ECP+CPP method, as reported in Ref. [28], contributes less than $\sim +0.20$ cm^{-1}.

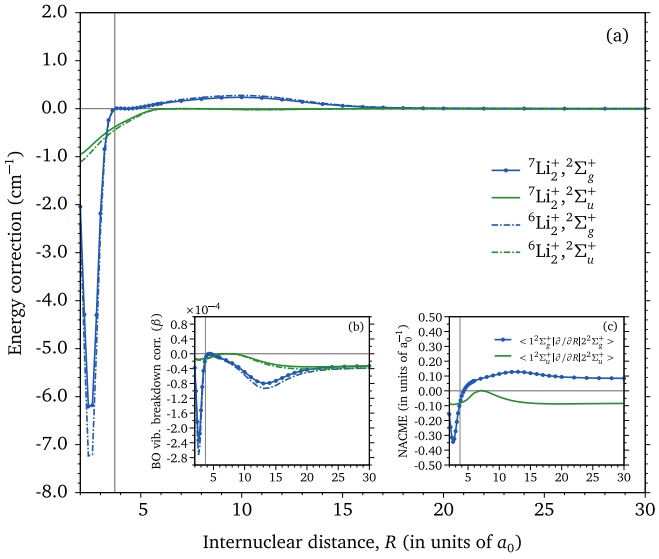

FIG. 8. (a) Energy corrections in the total energies, $-\beta(R)\times$PEC(R) (b) $\beta(R)$ parameters for $^7Li_2^+$ and $^6Li_2^+$, computed using Eq. (3) in Ref. [42] (c) NACME(R) for $\langle 1^2\Sigma_{g/u}^+ | \partial/\partial R | 2^2\Sigma_{g/u}^+\rangle$ for Li_2^+.

TABLE III. $^6Li^+$-^6Li and $^7Li^+$-^7Li scattering lengths a, computed for the $X^2\Sigma_g^+$ and $A^2\Sigma_u^+$ PECs without non-BO terms, are compared to the values obtained when the PECs are scaled with the κ factor (see text). Likewise, σ_{tot} at s-wave is also compared.

System, state	a (in a_0)	a^κ (in a_0)	Change
$^6Li_2^+, X^2\Sigma_g^+$	−874	−896	2.51%
$^6Li_2^+, A^2\Sigma_u^+$	−1355	−1363	0.59%
$^7Li_2^+, X^2\Sigma_g^+$	20465	16170	20.98%
$^7Li_2^+, A^2\Sigma_u^+$	1325	1317	0.60%
System	σ_{tot} (in a_0^2)	σ_{tot}^κ (in a_0^2)	Change
$^6Li_2^+$	1.41064×10^7	1.452×10^7	2.9%
$^7Li_2^+$	1.98396×10^9	1.2447×10^9	37.27%

With the aug-cc-pCV5Z basis sets and MRCI levels of electronic wave functions, it amounts to a similar order of change ($\sim +0.80\ cm^{-1}$).

Taking all these estimates into account, we see that the corrections to the BO-PECs are of the order of 1 cm^{-1}. To incorporate these corrections, we multiply the BO-PECs by $\kappa = +1.0001$ such that well depth, $D_e = 10458.58\ cm^{-1}$, of the BO-PEC for $^7Li_2^+(X^2\Sigma_g^+)$ increases by $1.045858\ cm^{-1}$. It is worth noting that the variation of the PECs in the large-R range $O(10^{-4})$, obtained by choosing this value of κ, covers well the variation observed from the uncertainty in C_4 [for $^7Li_2^+$, $\alpha_d = 164.1(6)$, $O(10^{-5})$] which determines the inaccuracy in the large-R range of the potentials.

We then solve the Schrödinger equation with the scaled PECs and calculate the scattering properties for both $^7Li_2^+$ and $^6Li_2^+$ systems. The scattering lengths are provided in Table III. The scattering lengths in all cases do not change their signs, when they are computed with the scaled PECs. The larger change in the scattering length for $^7Li_2^+, X^2\Sigma_g^+$ is due to the vicinity of a scattering pole [28], which makes the total s-wave cross section for the $^7Li^+$-^7Li system sensitive to small changes in the potential (see Table III). It is important to note that these relative changes, apart from $^7Li_2^+, X^2\Sigma_g^+$, are much smaller than the ones we accounted for to incorporate possible inaccuracy in the short-range potential (see in Ref. [28]). For example, in Ref. [28], the scattering length for $(^7Li_2^+, A^2\Sigma_u^+)$ was altered by $\sim \pm 7.5\%$, which is ten times larger than the variation observed with the inclusion of the non-BO corrections.

[1] A. Härter, A. Krükow, A. Brunner, W. Schnitzler, S. Schmid, and J. H. Denschlag, Phys. Rev. Lett. **109**, 123201 (2012).
[2] S. Haze, S. Hata, M. Fujinaga, and T. Mukaiyama, Phys. Rev. A **87**, 052715 (2013).
[3] W. W. Smith, O. P. Makarov, and J. Lin, J. Mod. Opt. **52**, 2253 (2005).
[4] A. T. Grier, M. Cetina, F. Oručević, and V. Vuletić, Phys. Rev. Lett. **102**, 223201 (2009).
[5] C. Zipkes, S. Palzer, C. Sias, and M. Köhl, Nature (London) **464**, 388 (2010).
[6] S. Schmid, A. Härter, and J. H. Denschlag, Phys. Rev. Lett. **105**, 133202 (2010).
[7] C. Zipkes, S. Palzer, L. Ratschbacher, C. Sias, and M. Köhl, Phys. Rev. Lett. **105**, 133201 (2010).
[8] S. Willitsch, M. T. Bell, A. D. Gingell, S. R. Procter, and T. P. Softley, Phys. Rev. Lett. **100**, 043203 (2008).
[9] C. Zipkes, L. Ratschbacher, C. Sias, and M. Köhl, New J. Phys. **13**, 053020 (2011).
[10] Z. Meir, T. Sikorsky, R. Ben-shlomi, N. Akerman, Y. Dallal, and R. Ozeri, Phys. Rev. Lett. **117**, 243401 (2016).
[11] I. Sivarajah, D. S. Goodman, J. E. Wells, F. A. Narducci, and W. W. Smith, Phys. Rev. A **86**, 063419 (2012).
[12] S. Dutta, R. Sawant, and S. A. Rangwala, Phys. Rev. Lett. **118**, 113401 (2017).
[13] T. Sikorsky, Z. Meir, R. Ben-Shlomi, N. Akerman, and R. Ozeri, Nat. Commun. **9**, 920 (2018).
[14] T. Feldker, H. Fürst, H. Hirzler, N. Ewald, M. Mazzanti, D. Wiater, M. Tomza, and R. Gerritsma, Nat. Phys. **16**, 413 (2020).
[15] J. Joger, H. Fürst, N. Ewald, T. Feldker, M. Tomza, and R. Gerritsma, Phys. Rev. A **96**, 030703(R) (2017).
[16] K. Ravi, S. Lee, A. Sharma, G. Werth, and S. A. Rangwala, Nat. Commun. **3**, 1126 (2012).
[17] S. Lee, K. Ravi, and S. A. Rangwala, Phys. Rev. A **87**, 052701 (2013).
[18] T. Dieterle, M. Berngruber, C. Hölzl, R. Löw, K. Jachymski, T. Pfau, and F. Meinert, Phys. Rev. A **102**, 041301(R) (2020).
[19] P. Weckesser, F. Thielemann, D. Wiater, A. Wojciechowska, L. Karpa, K. Jachymski, M. Tomza, T. Walker, and T. Schaetz, Nature (London) **600**, 429 (2021).
[20] S. Dutta and S. A. Rangwala, Phys. Rev. A **97**, 041401(R) (2018).
[21] A. Mahdian, A. Krükow, and J. H. Denschlag, New J. Phys. **23**, 065008 (2021).
[22] R. Côté and A. Dalgarno, Phys. Rev. A **62**, 012709 (2000).
[23] M. Li and B. Gao, Phys. Rev. A **86**, 012707 (2012).
[24] R. Côté, in *Advances In Atomic, Molecular, and Optical Physics* (Academic Press, Cambridge, MA, 2016), Vol. 65, pp. 67–126.
[25] D. S. Goodman, J. E. Wells, J. M. Kwolek, R. Blümel, F. A. Narducci, and W. W. Smith, Phys. Rev. A **91**, 012709 (2015).
[26] H. S. W. Massey and R. A. Smith, Proc. R. Soc. London A **142**, 142 (1933).
[27] M. R. C. McDowell and J. P. Coleman, *Introduction to the Theory of Ion-atom Collisions* (North-Holland Publishing Company, Amsterdam, 1970).
[28] A. Pandey, M. Niranjan, N. Joshi, S. A. Rangwala, R. Vexiau, and O. Dulieu, Phys. Rev. A **101**, 052702 (2020).
[29] L.-Y. Tang, Z.-C. Yan, T.-Y. Shi, and J. F. Babb, Phys. Rev. A **79**, 062712 (2009).
[30] P. Zhang, E. Bodo, and A. Dalgarno, J. Phys. Chem. A **113**, 15085 (2009).
[31] T. Schmid, C. Veit, N. Zuber, R. Löw, T. Pfau, M. Tarana, and M. Tomza, Phys. Rev. Lett. **120**, 153401 (2018).

[32] B. H. Bransden and M. R. C. McDowell, *Charge Exchange and the Theory of Ion-atom Collisions* (Clarendon Press, Oxford, 1992).

[33] E. Bodo, P. Zhang, and A. Dalgarno, New J. Phys. **10**, 033024 (2008).

[34] P. Zhang, A. Dalgarno, and R. Côté, Phys. Rev. A **80**, 030703(R) (2009).

[35] H. S. W. Massey, *Atomic and Molecular Collisions* (Taylor & Francis, London, 1979).

[36] E. W. McDaniel, *Collision Phenomena in Ionized Gases* (Wiley, New York, 1964).

[37] R. Côté and I. Simbotin, Phys. Rev. Lett. **121**, 173401 (2018).

[38] R. Côté, Phys. Rev. Lett. **85**, 5316 (2000).

[39] J. Grosser, T. Menzel, and A. K. Belyaev, Phys. Rev. A **59**, 1309 (1999).

[40] A. K. Belyaev, A. Dalgarno, and R. McCarroll, J. Chem. Phys. **116**, 5395 (2002).

[41] J. F. Stanton, J. Gauss, L. Cheng, M. E. Harding, D. A. Matthews, and P. G. Szalay, *CFOUR*, Coupled-Cluster techniques for Computational Chemistry, a quantum-chemical program package, with contributions from A. A. Auer, A. Asthana, R. J. Bartlett, U. Benedikt, C. Berger, D. E. Bernholdt, S. Blaschke, Y. J. Bomble, S. Burger, O. Christiansen, D. Datta, F. Engel, R. Faber, J. Greiner, M. Heckert, O. Heun, M. Hilgenberg, C. Huber, T.-C. Jagau, D. Jonsson, J. Jusélius, T. Kirsch, K. Klein, G. M. KopperW. J. Lauderdale, F. Lipparini, J. Liu, T. Metzroth, L.A. Mück, D. P. O'Neill, T. Nottoli, D. R. Price, E. Prochnow, C. Puzzarini, K. Ruud, F. Schiffmann, W. Schwalbach, C. Simmons, S. Stopkowicz, A. Tajti, J. Vázquez, F. Wang, J. D. Watts and the integral packages MOLECULE (J. Almlöf and P. R. Taylor), PROPS (P. R. Taylor), ABACUS (T. Helgaker, H. J. Aa. Jensen, P. Jørgensen, and J. Olsen), and ECP routines by A. V. Mitin and C. van Wüllen. For the current version, see http://www.cfour.de.

[42] F. Holka, P. G. Szalay, J. Fremont, M. Rey, K. A. Peterson, and V. G. Tyuterev, J. Chem. Phys. **134**, 094306 (2011).

[43] H.-J. Werner, P. J. Knowles, G. Knizia, F. R. Manby, and M. Schütz, WIREs Comput. Mol. Sci. **2**, 242 (2012); https://onlinelibrary.wiley.com/doi/abs/10.1002/wcms.82.